Journal of Nuclear Materials 392 (2009) 200–205

Contents lists available at ScienceDirect

Journal of Nuclear Materials

journal homepage: www.elsevier.com/locate/jnucmat

Radiation stability of ZrN under 2.6 MeV proton irradiation

Yong Yang [a,*], Clayton A. Dickerson [b], Todd R. Allen [a]

[a] Department of Engineering Physics, University of Wisconsin-Madison, WI 53706, USA
[b] Material Science Program, University of Wisconsin-Madison, Madison, WI 53706, USA

A B S T R A C T

Zirconium nitride is a promising alternative material for the use as an inert matrix for transuranic fuel, but the knowledge of the radiation tolerance of ZrN is very limited. We have studied the radiation stability of ZrN using a 2.6 MeV proton beam at 800 °C. The irradiated microstructure and hardening were investigated and compared with annealed samples. A high density of nano-sized defects was observed in samples irradiated to doses of 0.35 and 0.75 dpa. Some defects were identified as vacancy-type pyramidal dislocation loops using lattice resolution imaging and Fourier-filter image processing. A very slight lattice expansion was noted for the sample with a dose of 0.75 dpa. Hardening effects were found for samples irradiated to both 0.35 and 0.75 dpa using Knoop indentation.

Published by Elsevier B.V.

1. Introduction

Interest in nitride-based fuels has arisen within the advanced fuel cycle initiative (AFCI) of the US Department of Energy [1], and several authors proposed zirconium nitride as one of the most promising inert matrix materials based on superior thermal and neutronic characteristics [2–5]. In addition, the compatibility with sodium and solubility in nitric acid for ZrN has also been tested and confirmed [4]. ZrN based inert matrix fuels could potentially enhance proliferation resistance of next generation reactors and reduce the environmental impact of nuclear energy production via transmutation of transuranic fission products. ZrN has also been proposed as a surrogate material for developing, testing and characterization of transuranic fuel since it has an isostructure with many actinide mononitrides [6].

However, very little information concerning radiation tolerance of ZrN is available. Most of the reported research was using ion irradiations, such as He, Xe, and Kr ion bombardment at various temperatures [7,8]. Neutron irradiation was performed at moderate neutron fluence, but only the electrical resistivity was evaluated [9]. Like many transition-metal carbides and nitrides, stoichiometric ZrN has a $B1$ (NaCl) structure, consisting of two intercalated face-centered sub-networks. A strong covalent Zr–N bonding confers the refractory properties, while the variability in physical properties is reportedly due to the various stoichiometries, which can affect the electronic structure, intrinsic vacancy concentrations, and potentially the radiation damage structures [10,11].

The purpose of present study is to provide some fundamental insight into the radiation response of ZrN under a proton beam. The microstructural evolution at two different fluences with irradiation at 800 °C was analyzed and the microhardness changes were also evaluated.

2. Experimental

2.1. Materials

Commercial grade ZrN rods were obtained from CERCOM Inc. (Vista, California 92801). The material was produced by hot pressing of commercial powder from H.C. Stark Inc. (Newton, MA 02461). The ceramic was received as 25 mm long rods with a diameter of 3 mm. The density was measured as 7.06 g/cm^3 using an immersion method, and the ratio to the theoretical density 7.32 g/cm^3 shows 3.7 vol.% porosity in the material. The chemical composition determined by NSL Analytical Services, Inc. with ICP–MS and Leco methods, is listed in Table 1 [12]. The ratio of N/Zr is 0.803 and the material is sub-stoichiometric with a nitrogen-deficient sublattice. Impurities of O and C possibly originated from the ZrN power fabrication procedure, i.e., carbothermic nitridation of oxides.

2.2. Proton irradiation

The irradiations were performed with a 2.6 MeV proton beam using the UW Tandem Accelerator, and the desired irradiation temperature was reached via a combination of a heating stage with an attached Gaumer GB301X-500-CB cartridge heater and the proton beam heating. The damage profile, calculated using TRIM2008 (Transport of Ions in Matter) [13] with a threshold displacement

* Corresponding author. Tel.: +1 608 263 5444; fax: +1 608 263 7451.
E-mail address: yyang@cae.wisc.edu (Y. Yang).

0022-3115/$ - see front matter Published by Elsevier B.V.
doi:10.1016/j.jnucmat.2009.03.040

Table 1
Chemical composition of ZrN [12].

Element	Ti	Cr	Si	Hf	Fe	W	C	N	O	Ca	Mo	V	Sn	Zr
wt%	.095	0.034	.007	.015	<0.069	0.19	0.76	10.81	1.27	0.011	0.021	0.02	0.011	Bal.

energy (E_d) of 35 eV for zirconium and 25 eV for nitrogen, is shown in Fig. 1. The values of E_d are based on the estimation of ZrC [14], though the true values of E_d for Zr and N are not available. It is reasonable to assume that the value of E_d for N is nearly the same as that of C, and to assume that E_d for Zr atoms is 20–40 eV, which is typical for many metal atoms. The depth of greatest interest is the 'flat' region 10–25 μm before the peak and this region is where the damage, as given in displacements per atom (dpa) was calculated. The H^+ ion concentration is nearly negligible in this region. The damage rates were taken from the 'Full Damage Cascade' calculation condition in TRIM program, and the calculated dose rate is $\sim 1 \times 10^{-5}$ dpa/s. Two irradiations, to doses of 0.35 and 0.75 dpa, were performed on the samples at a temperature of 800 °C measured by the three stage-embedded thermocouples, and the uniformity of the experimental temperature across the samples was monitored using an infrared camera. The irradiation temperature deviations are ±23 and ±9 °C for the doses of 0.35 and 0.75 dpa, respectively.

2.3. Characterization

For comparison, the as received ZrN samples were also vacuum annealed at 800 °C for 20 h which corresponds to the time needed to accumulate 0.75 dpa at our irradiation conditions, and the related microstructure was fully characterized using scanning electron microscopy (SEM), transmission electron microscopy (TEM) and X-ray diffraction (XRD). For the irradiated samples, a thin layer of ~10 μm was removed from the irradiated surface to eliminate the free surface effects from the subsequent microstructural and mechanical property studies. The plan-view and cross-section TEM samples were prepared using wedge polishing followed by low angle ion milling, and for the plan-view specimen, the electron transparent area was controlled to be at the range around 20 μm below the irradiated surface. The TEM characterization was conducted using a Philips CM200UT TEM, and the possible radiation induced segregation along grain boundaries or the dislocation loops was examined using electron dispersive spectroscopy (EDS) with a spot size of 6 nm diameter. To study the lattice expansion caused by proton irradiation, X-ray Diffraction (XRD) was conducted using a STOE X-ray Powder Diffractometer. The hardening from proton irradiation was evaluated using a Knoop micro-indenter with a load of 50 g and 15 s load time. The sample surfaces were diamond lapped to 1 μm and finished with a ~0.04 μm silica final polish. The indentation penetration is ~2.5 μm which is only one tenth of the irradiated depth; the shallow impression effectively eliminates the influence of underlying damage peaks and unirradiated matrix materials and complies with the ASTM standard [15].

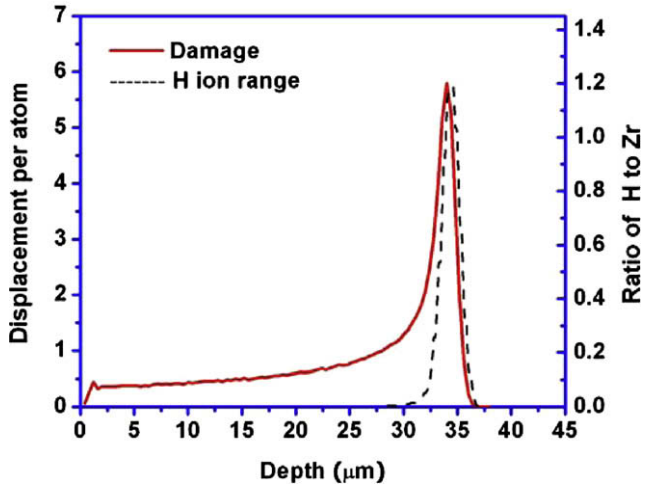

Fig. 1. Damage profile estimated with TRIM2008 in ZrN and concentration of implanted H (broken line), irradiated with 1×10^{19}/cm^2 2.6 MeV protons.

3. Results

3.1. Microstructure of as-annealed conditions

The SEM image in Fig. 2 shows the grain structure of the annealed ZrN. The material has a relative high porosity, especially at triple grain boundary junctions. A second phase was identified, indicated with arrows in Fig. 2. It contains ~57 at% oxygen with the balance zirconium, and is identified as Zr_xO_y using EDS.

The TEM microstructure of annealed ZrN is shown in Fig. 3. In general the material is nearly free of dislocation lines or networks, but some dislocation lines can be found in the vicinity of submicron-sized precipitates as shown in Fig 3(c). Significant numbers of heavily twinned oxides were observed at the triple grain boundary junctions as shown in Fig 3(b), which was consistent with the mix of monoclinic, tetragonal and cubic phases found in ZrN by Egeland using glancing angle XRD [7]. Additionally, clusters of faceted voids were observed in some grains, and high resolution TEM (HRTEM) revealed the existence of a thin layer of an amorphous Si_xO_y at the edge of the voids. Diamond shaped voids were also found by Wheeler et al. in ZrN annealed at 1400 °C in a N_2–6%H_2 environment. However, the formation mechanism of these voids has not been positively determined, and sintering and annealing conditions definitely can affect the microstructure and mechanical properties [6].

3.2. Characterization of irradiated ZrN

The irradiated microstructures were characterized using bright field (BF), weak beam dark field (WBDF) and HRTEM at or near the zone axis [011]. The microstructure of annealed and irradiated

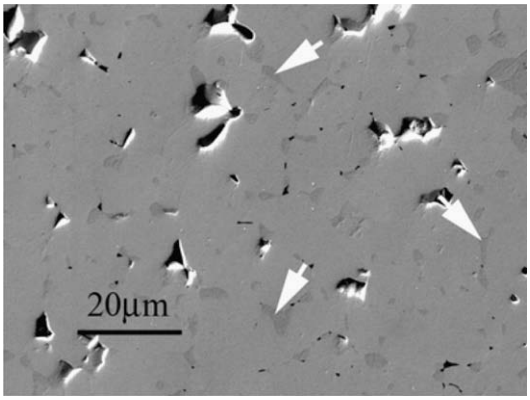

Fig. 2. SEM image of annealed ZrN, the second phase is identified as Zr_xO_y.

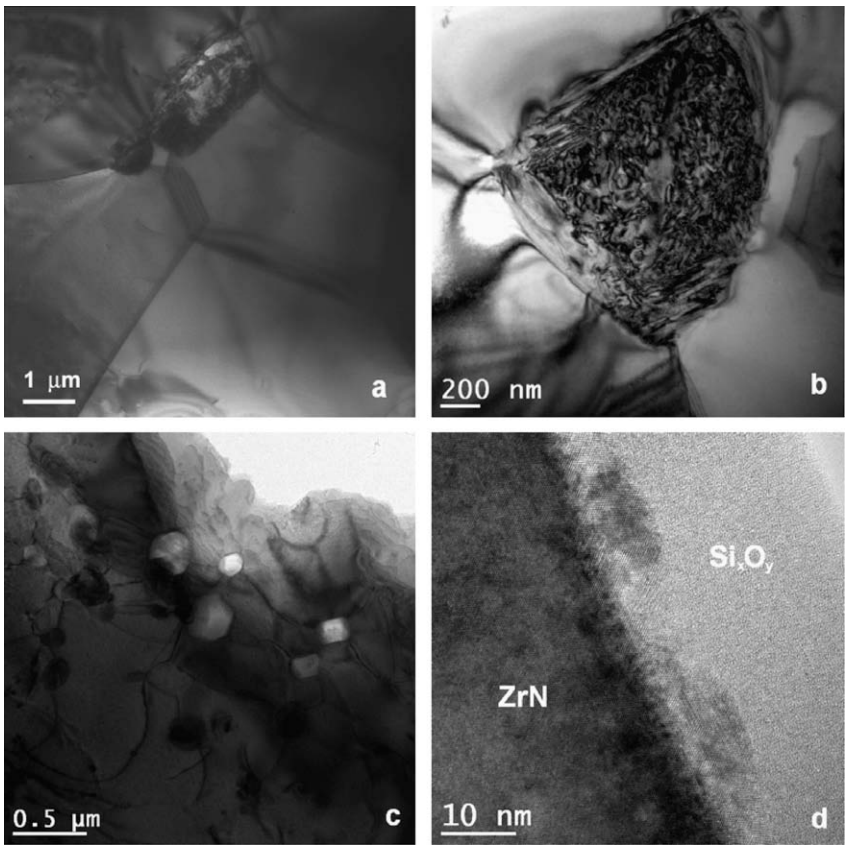

Fig. 3. (a) General view of the microstructure of ZrN; (b) Heavily twinning of Zr_xO_y phase at triple boundary junction; (c) Faceted voids and submicron-sized precipitates of Zr_xO_y observed in some grains; (d) HRTEM shows the amorphous Si_xO_y at the edge of voids.

material is compared in Fig. 4. No radiation induced nano-sized voids or bubbles were observed for dose levels of 0.35 or 0.75 dpa using the through-focus technique, and no amorphization was observed.

From Fig. 4 (b)–(e), it can be noted that the irradiated microstructures are dominated by nano-sized black spots and streaks. Compared with the 0.35 dpa irradiation, a dose of 0.75 dpa produced a higher density of defects, but the sizes of defects are still in a similar range. Although, the Moiré fringes associated with the defects can already be observed in the 0.35 dpa irradiated sample, they became more pronounced in the microstructures irradiated to 0.75 dpa. The same feature was also observed in Kr-irradiated samples and it was postulated they resulted from the overlap of a ZrO_2 films formed during irradiation [8]. However, since EDS is not sensitive enough to detect oxygen concentrations in the Moiré fringes spot regions, the final conclusion needs to be further investigated with Z contrast imaging and EELS technologies.

Fig. 5 shows that the irradiated microstructure is very different from that previously studied in proton irradiated ZrC. The diffraction pattern of the irradiated ZrN at a 2-beam condition with $g = 31\bar{1}$ near the [011] zone axis does not reveal any rel-rod streaks, which are often used to image the faulted dislocation loops lying on the four {111} planes in materials with an fcc structure [16,17]. Therefore for the irradiated ZrN, there are much lower densities of faulted dislocation loops than in ZrC. The differences may be caused by the different ionic-covalent bonding. There is a lower tendency for localization of electrons near the Zr core in the nitride than in the carbide [18]. The much higher initial vacancy concentration on the N sublattice may also favor different defect structures.

To explicitly identify the nature of the defects observed in irradiated ZrN, the lattice image was analyzed using Fourier-filtering. Fig. 6 shows an image of a typical planar-like defect projected as streaks along the $B = [011]$ direction. After masking the 200 diffraction spots and applying inverse Fourier transformation, a pyramidal dislocation loop is clearly displayed. As shown in Fig. 6(c), the dislocation loops appear as two opposite-sign dislocations (dipole) between which there exists a region of lattice distortion. Note that these two dislocations are spaced only at a distance of approximately four (200) planes and the defect appears as vacancy-type. However, it should be noted that lattice images are obtained from very localized and thin regions of the sample (<20 nm thick) and the images are very sensitive to sample thickness and microscope settings. Individual images may not represent the real feature and certainly not the entire characteristics. Further experimental work is needed to identify the vacancy pyramidal plane condensation mechanism in irradiated ZrN.

To examine the irradiation damage along the proton penetration depth, TEM images were taken on cross-sectional samples. To illustrate more clearly, an optical image of the cross-sectioned irradiated ZrN sample is shown in Fig. 7, and it can be seen that there is a very sharp crack line located near the position of the radiation damage peak calculated using TRIM. The detail of the crack line is shown clearly in Fig. 8, and it can be seen that the crack may have formed from the coalescence of aligned voids, and three more lines of small voids can be seen parallel to the crack and perpendicular to the proton beam direction. It seems that the voids were aligned by the proton beam front and moved forward along the irradiation direction and stop at the peak of the damage profile. Additionally, based on the crystal orientations on both sides of the crack, it was found that the crack is transgranular instead of intergranular. The void surfaces and the material interconnecting the voids on the crack line were revealed as silicon rich oxides shown

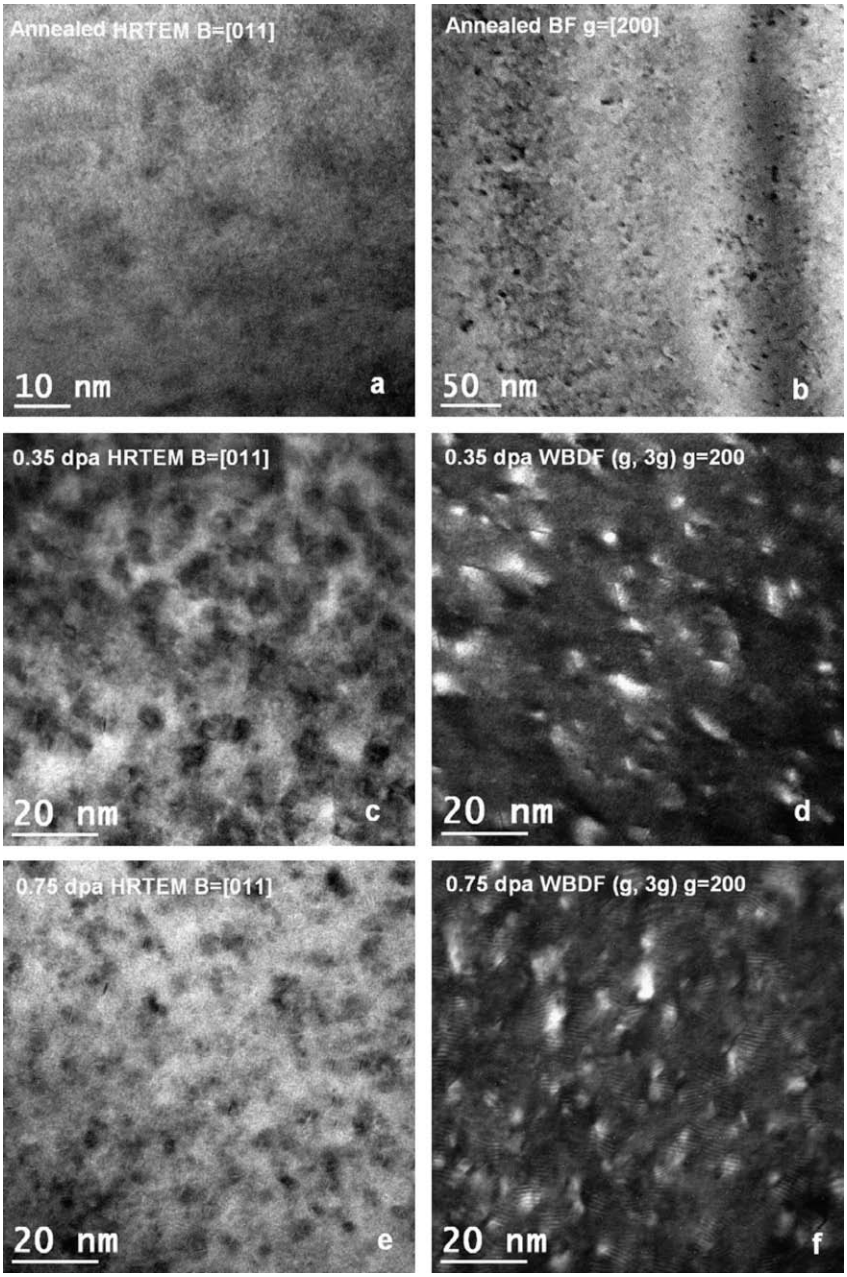

Fig. 4. BF, DF, and HRTEM images of as-annealed and irradiated ZrN: (a) and (b) annealed ZrN; (c) and (d) sample irradiated with 0.35 dpa with average loop size of 2.23 nm and density of 8.36×10^{15} m^{-2}; (e) and (f) sample irradiated with 0.75 dpa with average loop size of 2.35 nm and density of 1.12×10^{16} m^{-2}.

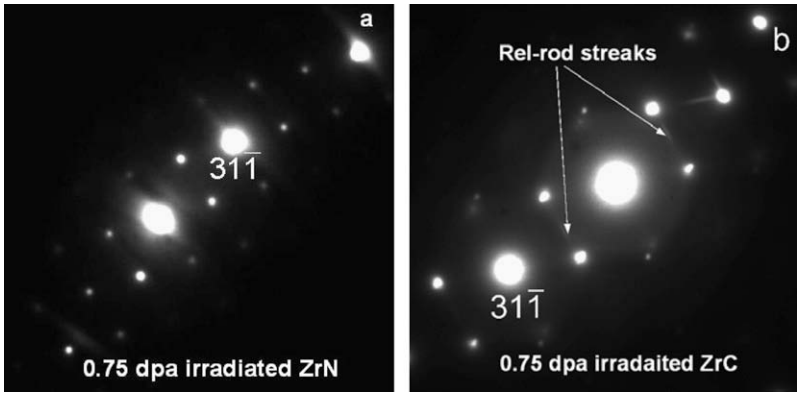

Fig. 5. Two-beam condition diffraction pattern with $g = 31\bar{1}$ near zone axis [0 1 1]: (a) 0.75 dpa irradiated ZrN and (b) 0.75 dpa irradiated ZrC [17].

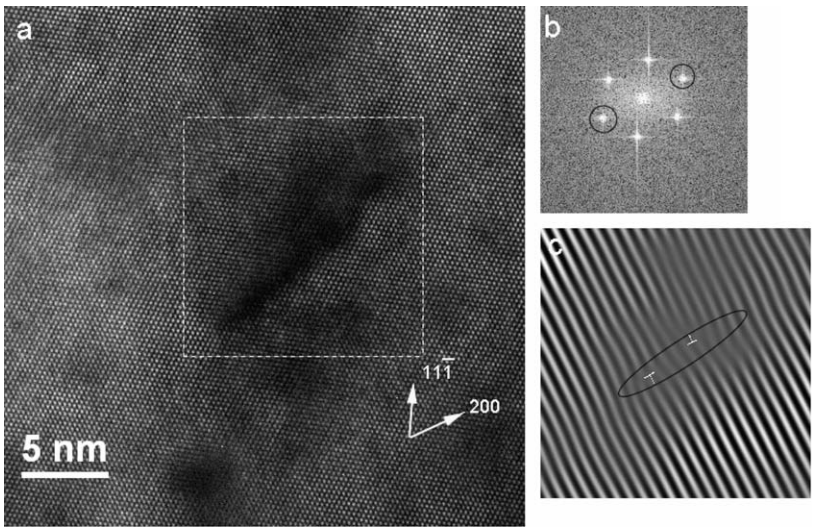

Fig. 6. (a) [011] lattice image of planer like defect; (b) Fourier transformation of selected area; (c) Fourier-filtered (200) diffraction lattice images revealing the pyramidal dislocation loops.

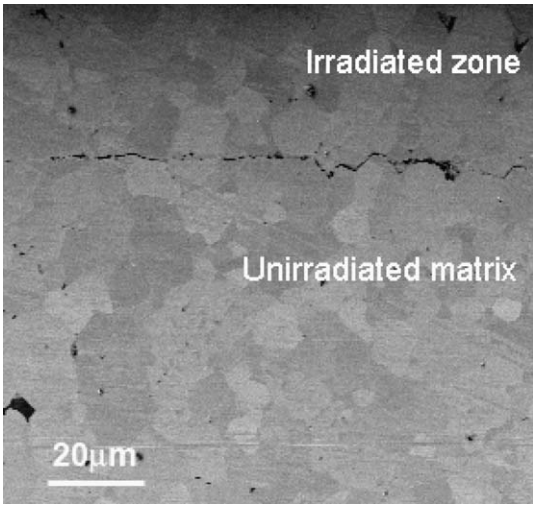

Fig. 7. Optical image of the cross-section of irradiated ZrN.

by the EDS spectrum in Fig. 8(b). However, the mechanism of the Si segregation to the aligned voids caused by the proton irradiation is unclear. Additionally, any hydride formation especially near the damage peaks needs to be further studied.

3.3. Lattice expansion

The lattice expansion was measured using X-ray diffraction. To eliminate the error induced by any possible misalignment during the X-ray diffraction setup and to obtain more accurate lattice parameters, a thin layer of alumina was deposited on the sample surfaces as a reference marker. As listed in Table 2 for the 0.35 dpa irradiated sample, there is no noticeable lattice variation from the unirradiated value, since the difference falls within the range of measurement error. For the 0.75 dpa, a slight lattice expansion was observed. This measurement is consistent with our HOLZ evaluation, which shows no noticeable changes in the HOLZ patterns of irradiated samples compared with the unirradiated.

3.4. Irradiation hardening

Irradiation hardening was evaluated using Knoop micro-indentation. The increase of the microhardness due to proton irradiation is 9.5% for 0.35 dpa and 14.6% for 0.75 dpa, shown in Fig. 9. Irradiation hardening in ceramics is mainly attributed to the formation

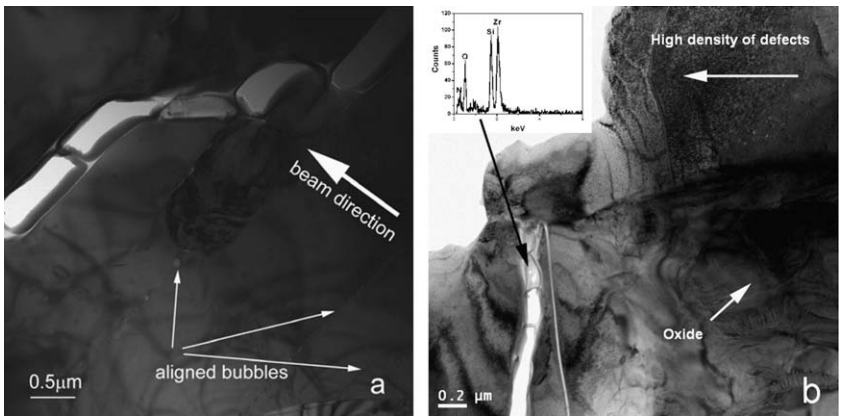

Fig. 8. TEM image of cross-section sample of irradiated ZrN with dose of 0.75 dpa: (a) aligned bubbles perpendicular to the proton beam direction; (b) Crack lines formed from the coalescence of aligned voids, and silicon rich oxides on the voids surface was identified using EDS.

Table 2
Lattice variation in ZrN for different irradiated conditions.

Condition	Lattice constant (nm)	Lattice variation (nm)	Std. Dev. of mean (nm)
Annealed	0.458353	–	0.000601
0.35 dpa	0.458237	−0.000160	0.000237
0.75 dpa	0.458696	+0.000343	0.000147

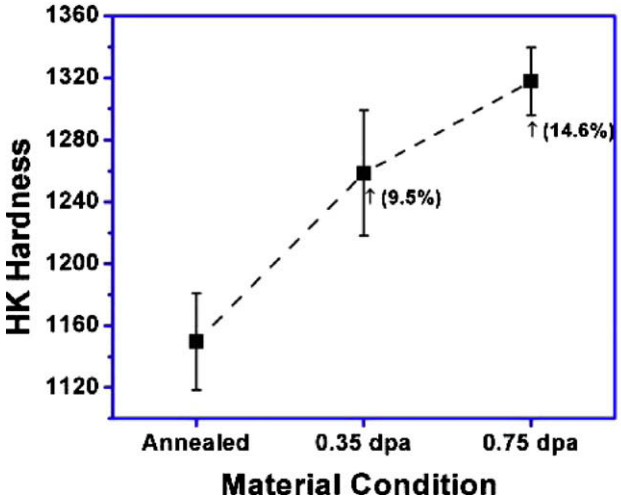

Fig. 9. Knoop hardness of ZrN with different irradiation conditions (15 indents were measured for each condition, and error bars denote the standard error of mean).

of point defects [19,20]. The strain fields around point defects interact with dislocations during deformation and act as a pinning center and the point defects also play an important role in dynamic processes such as crack propagation. Hardening due to irradiation had been studied in Al_2O_3, $MgO + 3Al_2O_3$, $MgAl_2O_4$, AlN, and SiC using the indentation method, and the mechanism of hardening has been clarified particularly in spinel [19–21]. As an example, when AlN was irradiated by Iseki at 470 °C to a fluence of 2.4×10^{24} neutrons m^{-2}, a large number of small dislocation loops were observed and the microhardness increased by ~51%. After annealing at 1400 °C, the microstructure still contained a large number of small dislocation loops, but the hardness recovery was almost complete, as was the swelling recovery which was caused by point defects. Therefore, it was concluded that point defects and small defect clusters cause the hardening, while relatively large dislocation loops may play little role in the hardening [20]. Further annealing experiments with irradiated ZrN are planned to study microstructure and hardening.

4. Conclusion

Proton irradiation of ZrN at 800 °C produced no radiation induced voids or bubbles for a dose up to 0.75 dpa. Crack lines and aligned bubbles were observed in the vicinity of the irradiation damage peak which has a much higher dose level and concentration of stopped hydrogen. No irradiation induced amorphization or precipitates were detected at a dose of 0.35 or 0.75 dpa. The irradiated microstructures are dominated by a high density of dislocation loops and point defects, and lattice resolution TEM images show some of the loops are vacancy-type in nature. Compared with the 0.35 dpa sample, the average size of the defects in the 0.75 dpa sample remains nearly constant but the density increased. Only a very slight lattice expansion was observed for the 0.75 dpa irradiated sample; for the 0.35 dpa sample, the lattice change falls into the range of measurement error.

Radiation hardening was found for doses of 0.35 and 0.75 dpa and this hardening is attributed to the formation of point defects. However, further annealing experiments on the irradiated sample are needed to make firm conclusions on the mechanism of radiation hardening in ZrN.

Acknowledgement

This work is funded by the US Department of Energy through Nuclear Energy Research Initiative program (Project 06-007 and Award #DE-FC07-06ID14740).

References

[1] AFCI Program Plan, 2005.
[2] M. Streit, F. Ingold, J. Eur. Cer. Soc. 25 (2005) 2687.
[3] K. Minato, M. Akabori, M. Takano, Y. Arai, K. Nakajima, A. Itoh, T. Ogawa, J. Nucl. Mater. 320 (2003) 18.
[4] M. Burghartz, G. Ledergerber, H. Hei, R.R. van der Lann, R.J.M. Konings, J. Nucl. Mater. 288 (2001) 233.
[5] M.K. Meyer, N. Chauvin, in: Proceedings of GLOBAL2003, New Orleans, Louisiana, USA, 16–20 November 1990.
[6] K. Wheeler, P. Peralta, M. Parra, K. McClellan, J. Dunwoody, G. Egeland, J. Nucl. Mater. 366 (2007) 306.
[7] G.W. Egeland, PhD thesis, 2005.
[8] J. Gan, R.S. Fielding, M.K. Meyer, R.C. Birtcher, FY-2005 Summary Report, INL, 2005.
[9] M.L. Taubin, Soviet Atomic Energy 69 (3) (1990) 176.
[10] H. Hochst, R.D. Bringans, R.L. Johnson, Annals Israel Physical Soc. 6 (1984) 336.
[11] V.A. Lavrenko, V.A. Shvets, A.D. Panasyuk, L.I. Kuznetsova, Power Met. Metal Ceram. 42 (2003) 419.
[12] Report, INL/EXT-06-11749, September 2006.
[13] J.F. Ziegler, J.P. Biersack, U. Littmark, The Stopping and Range of Ions in Solids, Pergamon Press, New York, 1996.
[14] D. Gosset, M. Dollé, D. Simeone, G. Baldinozzi, L. Thomé, J. Nucl. Mater. 373 (2008) 123.
[15] ASTM Standard: C 1326-03, Standard Test Method for Knoop Indentation Hardness of Advanced Ceramics, 2003.
[16] D.J. Edward, E.P. Simonen, S.M. Bruemmer, J. Nucl. Mater. 317 (2003) 13.
[17] Y. Yang, C.A. Dickson, H. Young, B. Miller, T.R. Allen, J. Nucl. Mater. 378 (2008) 341.
[18] NASA Technical Note-3533, 1966.
[19] H. Suematsu, H. Iseki, T. Yano, Y. Saito, T. Suzuki, T. Mori, J. Am. Ceram. Soc. 75 (1992) 1742.
[20] S.J. Zinkle, J. Am. Ceram. Soc. 72 (1989) 1343.
[21] T. Iseki, M. Tezuka, C. Kim, T. Suzuki, H. Suematsu, T. Yano, J. Nucl. Sci. Techol. 30 (1993) 68.